**Proceedings of the ASME 2018 37th International Conference on Ocean, Offshore & Arctic Engineering**
**OMAE2018**
**June 17-22, 2018, Madrid, Spain**

# OMAE2018-78534

# DRAG COEFFICIENTS OF VERTICALLY-MOUNTED FULL-SCALE BLUE MUSSEL DROPPER LINES

**Arndt Hildebrandt***
Ludwig-Franzius-Institute for Hydraulic, Estuarine and Coastal Engineering
Hannover, Lower Saxony, Germany

**Jannis Landmann**
Ludwig-Franzius-Institute for Hydraulic, Estuarine and Coastal Engineering
Hannover, Lower Saxony, Germany

**Thorsten Ongsiek**
Ludwig-Franzius-Institute for Hydraulic, Estuarine and Coastal Engineering
Hannover, Lower Saxony, Germany

**Nils Goseberg**
Leichtweiß-Institute for Hydraulic Engineering and Water Resources, Department of Hydromechanics and Coastal Engineering
Brunswick, Lower Saxony, Germany

## ABSTRACT

*Developments in marine aquaculture in the last 30 years indicate that the bivalve-related industry is feasible offshore and that opportunities for large-scale, industrious production of shellfish stock exists. The objective of the project "CAWX1607" is to develop, model and test such systems. However, the forces acting on suspension cultures, the most likely form of marine farm systems are unknown. Here, drag coefficients provide an efficient approach for the calculation of arbitrary complex structures by using the Morison equation. The $C_D$-coefficients take into account vortex shedding effects as well as the surface roughness of the structure.*

*This paper reports on developed and conducted tests at the medium wave and towing tank "Schneiderberg" (WKS) at the Ludwig-Franzius-Institute for Hydraulic, Estuarine and Coastal Engineering of the Leibniz University Hanover, Germany. The tests were conducted for current velocities between 0.25 – 1.0 m/s for three samples of blue-lipped mussel specimens. During physical testing the forces and moments in x-,y- and z-direction, the elevation of the water surface, a velocity profile in the vicinity of the live-blue mussels, as well as the velocities of the towing carriage were recorded. The developed methodology, data treatment as well as the resulting $C_D$-coefficients are presented. Further, the $C_D$-coefficients obtained are presented in the context of natural variation of living structures and discussed in comparison to $C_D$—curve characteristics of offshore structures, e.g. rough cylinders.*

## KEYWORDS

Drag coefficient, aquaculture, dropper lines, Morison equation, physical modelling

## NOMENCLATURE

| | | |
|---|---|---|
| $D_i$ | Characteristic linear dimension | [m] |
| $\rho_{water}$ | Density of water | [kg/m³] |
| $C_D$ | Drag coefficient | [-] |
| $F_D$ | Drag force | [N] |
| $\dot{u}$ | Flow acceleration | [m/s²] |
| $F_x$ | Force in x-direction | [N] |
| $F_y$ | Force in y-direction | [N] |
| $F_z$ | Force in z-direction | [N] |
| $C_M$ | Inertia coefficient | [-] |
| $\nu$ | Kinematic viscosity | [m²/s] |
| $M_x$ | Moment in x-direction | [Nm] |
| $M_y$ | Moment in y-direction | [Nm] |
| $M_z$ | Moment in z-direction | [Nm] |
| $A$ | Referential area | [m²] |
| $Re$ | Reynolds number | [-] |
| $L_{wet}$ | Submerged/wetted length | [m] |
| $u_i$ | Test velocity i | [m/s] |
| $t$ | Time | [s] |
| $V$ | Volume of the observed body | [m³] |
| $H$ | Wave Height | [m] |
| $T$ | Wave Period | [s] |

* Corresponding author

## INTRODUCTION

Bivalve-related aquaculture is a long-standing staple of human alimentation. From uncultivated harvesting, i.e. gathering of naturally attainable bivalve stock, to industrialized farming, which includes catching mussel larvae during their free-floating "spat" stage. All in all, 5.6 % of all aquaculture production worldwide is of bivalve origin which represents 16 million tons (FAO, 2016). The ever-increasing demand for hydroponic products further indicates that aquaculture will continue to be one of the fastest-growing sectors for protein-based food production (FAO, 2016). Although, the perspectives for aquaculture are favorable operates shellfish-related aquaculture currently mostly in calmer, near-shore conditions. Consequently, offshore operations and aquaculture growing will take place at remote and wave energetic locations in the near future, due to the increasing demand for marine proteins (Buck et al., 2010). The reasons for turning to offshore aquaculture range from the reduction of conflicts between stakeholders in nearer coastal waters, to the ample space available for expansion and reduced exposure to pathogenic pollution (Buck and Krause, 2012), to being able to use large volumes of high quality water to decrease the stress on cultured organisms or the economic demand to create revenue by offsetting seafood deficits (McVey, 1996).

The feasibility of moving bivalve-related aquaculture to high-energy environments is often connected to already existing offshore structures. Nonetheless, the connection of aquaculture farming concepts to those structures is still at an early stage (Buck and Krause 2013, van den Burg et al., 2013; Lagerveld et al., 2014; Carlberg and Christensen, 2015). Depending on the site conditions, different aspects have to be considered as aquaculture design will always be governed by the specific environment, in-, near- or off-shore. Especially at off-shore sites, larger forces are exerted on the structures for farming and processing due to wave and current action. Although hydrodynamic forces acting on fixed (Hildebrandt & Sriram 2014), floating (Welzel et al. 2016), and cylinder grouped structures in such conditions are commonly investigated (Hildebrandt et al. 2009), existing research related to shellfish aquaculture is scarce. Flow analysis around mussels is part of current research activities, however mainly focusing on naturally bedded mussel cultures (Constantinescu et al., 2013; Sansom et al, 2017) or on netted structures in association to biofouling (Gansel et al., 2017) in contrast to suspended long-line systems which would be used primarily in offshore conditions. Little is known about the forces acting on dropper lines and the corresponding mooring and buoyancy devices in off-shore conditions. To date, primarily technological approaches to the topic itself are researched (Goseberg et al., 2017). Thus, experimental research is used in this study to address research gaps regarding the behavior of suspended long-lines in current and wave conditions.

A series of physical tests with full-scale blue mussel dropper lines was conducted to assess the corresponding drag and inertia characteristics as well as to estimate the magnitude of wave and current forces acting on the mussel dropper lines (Landmann et al., 2018).

This paper focuses on the estimation of drag force coefficients for constant current loads based on the analyzed experiments. To this end the Morison equation (Morison et al., 1950) and the $C_D$ coefficient are used to quantify the drag loads on mussel dropper lines for various current velocities. The data processing is presented with a special emphasis on the isolation of the loads acting on the blue mussel dropper lines. Furthermore, the resulting drag coefficients for different velocities are presented and discussed regarding their sensitivity to model parameters, i.e. the referential area $A$. Finally, the results are discussed in the context of natural variations of living structures and compared to $C_D$—curve characteristics of rough offshore cylinders for reference.

The developed and performed physical model tests, as well as the associated numerical calculations and the ongoing research efforts are further used and combined to determine wave forces acting on bivalve-based aquaculture systems.

## METHODOLOGY

Tests of the live-mussel specimens were carried out at the medium wave and towing tank "*Schneiderberg*" (WKS) at the Ludwig-Franzius-Institute for Hydraulic, Estuarine and Coastal Engineering of the Leibniz University Hanover, Germany. The WKS is 110 m long, 2.2 m wide and holds up to 1.1 m water with a total depth of 2.0 m. Regular and irregular waves can be generated with up to 0.5 m wave heights. A towing carriage allows for testing at constant velocities of up to 1.5 m/s. Three samples of blue mussel dropper line as well as the test frame without an attached specimen were tested with four different velocities up to 6 repetitions to obtain the data basis to analyze the drag characteristics. Figure 1 depicts the test frame and the attached measuring equipment. Figure 2 illustrates the mussels used for testing and exhibits the highly irregular surface of the tested specimens. For a more detailed description of the assembled test frame, the test conditions, the test program as well as the tested live mussel specimens see Landmann et al. (2018).

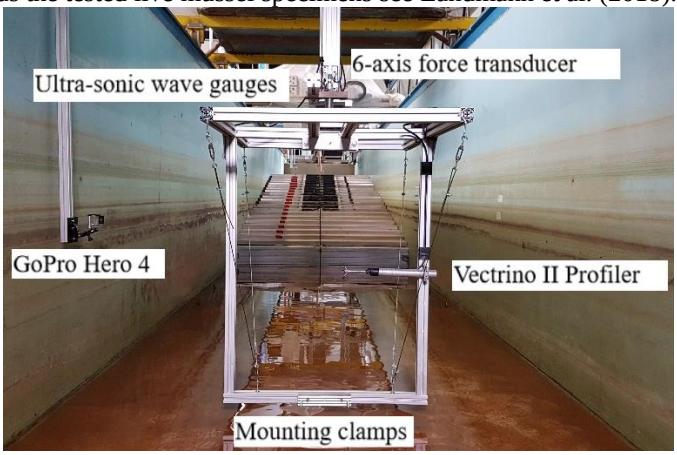


*Figure 1: Test frame with underwater camera, Vectrino II Profiler, ultra-sonic wave gauges and mounting clamps without attached blue mussel specimen*

*Figure 2: Blue mussel (Mytilus edulis) dropper line specimen 1 during preparation for drag testing.*

The tests referred to in this paper concentrate on the top- and bottom-mounted drag tests and the corresponding frame-only tests (FOT). Due to the towing test set-up a uniform velocity distribution throughout the water column is produced acting on the whole dropper line that were pre-tensioned as described in Landmann et al. (2018). Thus the deformation of the lines could be kept at a minimum, with a deflection of the midsection of the mussel dropper line of about 2 cm for the highest velocities.

For the identification of the drag characteristics of blue mussel dropper lines the time series of the force in x-direction $F_x$ and the corresponding velocity of the towing carriage $u_i$ are substituted into the drag term of the Morison et al. (1950) equation to determine the drag coefficient $C_D$:

$$F = \frac{1}{2}\rho C_D u^2 A + \rho C_M V \dot{u} \quad (1)$$

with $F$ the total horizontal force acting on front face of a structure, $\rho = 1000\frac{kg}{m^3}$ the density of fresh water, $C_D$ the drag coefficient, $u$ the horizontal particle velocity, $A = L_{wet} * D_i$ the referential area composed of the wetted length of tested structure $L_{wet}$ and the characteristic diameter $D_i$, $C_M$ the inertia coefficient, $V$ the volume of the structure and $\dot{u}$ the flow particle acceleration. The wetted length $L_{wet} = 0.80\ m$ is the same for all specimen as water level and the position of the test frame remain unchanged during testing. The first term of equation (1) corresponds to the acting drag forces, while the second term describes the inertia forces contributed by accelerated flows, which is neglected in this study. Thus, the first term is:

$$F_D = \frac{1}{2}\rho C_D u^2 A \quad (2)$$

with $F_D$ as the drag force acting on the body. The drag coefficient $C_D$ is described as:

$$C_D = \frac{2 * F_D}{\rho u^2 A} \quad (3)$$

and referenced to the dimensionless Reynolds number $Re$, expressed as:

$$Re = \frac{u * D_i}{\nu} \quad (4)$$

with $u$ being the velocity of the current or the towing carriage, $D_i$ a characteristic diameter of the observed body similar to Equation (1) and $\nu$ the kinematic viscosity of the fluid.

The current velocities achieved via the carriage are 0.25 m/s, 0.50 m/s, 0.75 m/s and 1.00 m/s. These velocities and the characteristic diameters of each specimen correspond to the Reynolds numbers $2.4 \times 10^4$ to $1.1 \times 10^5$, which covers the transition from laminar to turbulent flow of cylinders with a rough surface area comparable to the here tested mussel dropper lines (Achenbach, 1971).

Table 1 lists the tested range of Reynolds numbers and the corresponding velocities, while Table 2 lists the mean diameter of the tested specimens, the length of each tested specimen as well as the number of repetitions that were performed with each mussel dropper line. Specimen 1 shows natural variations regarding the diameter along its length as can be seen in Figure 2 that lead to a reduced diameter $D_i$ in contrast to the other specimens, which were more uniformly covered with mussels.

The characteristic diameter $D_i$ is determined through a 3D-scan of the different dropper line specimen. The visible area in direction of travel is subdivided into layers of 5 cm and the cumulated widths are used to calculate a mean diameter for every specimen.

For specimens 2 and 3 the repetitions were reduced to 2 – 6 repetitions to allow for quicker laboratory tests, as the live-mussels lose their cohesive properties when exposed to non-autochthonous conditions over prolonged times.

*Table 1: Overview of tested range of Reynolds numbers and corresponding velocities in m/s*

| **Reynolds numbers** | $2.4 \times 10^4$ to $3.6 \times 10^4$ | $5.0 \times 10^4$ to $6.2 \times 10^4$ | $7.0 \times 10^4$ to $9.0 \times 10^4$ | $9.8 \times 10^4$ to $1.1 \times 10^5$ |
|---|---|---|---|---|
| **Velocity** | 0.25 m/s | 0.50 m/s | 0.75 m/s | 1.00 m/s |

*Table 2: Overview regarding number of test repetitions, as well as length and diameter of each individual specimen in cm listed per specimen and for the Frame-Only-Tests (F.O.T.)*

| | **Specimen 1** | **Specimen 2** | **Specimen 3** | **F.O.T** |
|---|---|---|---|---|
| **Rep.** | 6 | 2 - 6 | 2 - 6 | 2 |
| $\boldsymbol{D_i}$ | 10.41 cm | 11.12 cm | 10.96 cm | - |
| **L** | 105 cm | 105 cm | 104 cm | - |

## DATA ANALYSIS

The raw data includes interfering influences like vibrations of the towing carriage as well as oscillations of the test frame itself, which is why the data is filtered initially. In a first step the

raw data is unified regarding the sample rate, which is chosen at 100 Hz. The data of the six-axis-force-transducer was sampled at a different rate than the rotary encoder, profiling velocimeter and the ultrasonic wave gauges due to device restrictions. The data sets are analyzed via Fast-Fourier-Transformations to identify frequency components that are associated with carriage motions and signal noise for example. An eight order lowpass-butterworth-filter with a cut-off frequency of 5 Hz is applied to all data sets to eliminate high frequent noise and towing carriage vibrations. Under water videos show that a cut-off frequency of 5 Hz is reasonable, since the motions of the specimen are dominated by lower frequencies.

The forces in x-direction $F_x$ of all data sets and corresponding velocities are plotted to easily assess their comparability, exemplarily shown in Figure 3 for tests with a velocity of 0.50 m/s. The consistent velocity around the desired value for all six test repetitions of this specimen as well as similar forces measured around 37 N acting on the blue mussel dropper line are discernible.

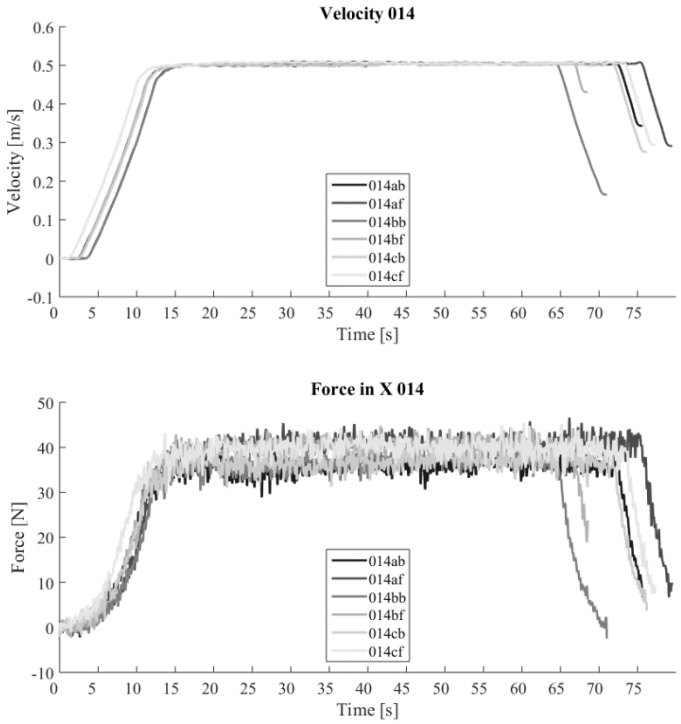


*Figure 3: Plausibility check for 0.50 velocity tests for test specimen 1 (014af, etc.).*

Similarly, for the test velocity $u_i$ all data sets of similar Reynolds numbers are compared. Furthermore, the velocity of the towing carriage is compared to the data of the profiling velocimeter attached to the test frame for plausibility. Three data sets of the profiling velocimeter, are related to the rotary encoder. Matching results regarding the velocity are discernible for all three measuring points. This suggests that the data points chosen are undisturbed by specimen induced turbulence and no shear-layer effects are to be expected in the measuring data closest to the profiling velocimeter. The medians of rotary encoder and profiling velocimeter data are created and compared to each other excluding acceleration and deceleration parts. The profiling velocimeter is subjected to vibration influences induced by the moving towing carriage, which is why the data from the rotary encoder is used for the uniform velocity information and computation of drag coefficients $C_D$ while the profiler data will be used for more detailed analysis of the flow in the near field of the mussels.

The next procedural step separates the force contribution of the test frame from the force contribution of the mussel dropper lines. If the velocity of the frame-only tests (FOT) and the specimen tests is equal, a simple subtraction of the FOT-forces suffices to obtain the forces needed. However, not all velocities were matched in FOT-testing. Thus, a $C_D$-dependent mathematical adjustment of the FOT-forces is necessary. As seen in Figure 4, Equation (3) is solved for all FOT-cases and the resulting $C_D$-coefficients are connected via an equation, here expressed as the red line. For unmatched velocities and thus Reynolds numbers, the $C_D$-coefficient can be estimated and Equation (2) is solved for all unknown values of $F_{Frame}$. In this way the quadratic influences of the velocity on the force can be accounted for and the influence of the test frame on the forces acting on the mussel dropper lines is minimized for all matched and unmatched velocities. The reduction of the forces guarantees that only the $C_D$-coefficients of the blue mussel dropper lines are accounted for and not the surrounding test equipment.

The subtracted forces are the median values of the FOT-tests between acceleration and deceleration periods. The median was chosen to negate the influence of outliers in the time series. For the given Reynolds-ranges in Table 1 reduction forces between 2.84 N and 100.73 N are computed.

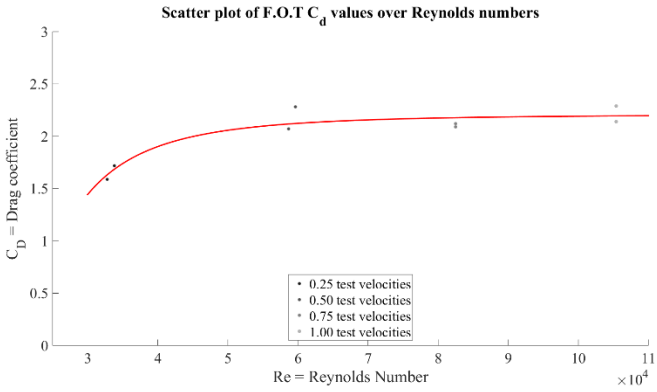


*Figure 4: FOT-related $C_D$-coefficients related to Reynolds numbers with fitted line for estimation of Reynolds numbers not included in the frame only tests and associated velocities.*

Subsequently, Equation (3) can be solved for all cases of Table 1. A single $C_D$-coefficient is determined for each sampled time step, which results in time dependent $C_D$-values for each test. The resulting $C_D$-coefficients are sorted in a descending and normalized in regard to their order, not altering the Cd-values but displaying the total distribution of values in a normalized scale and displayed in Figure 5. Here, the sorted distribution of the 1.0

m/s velocities and corresponding Reynolds range from $9.8 \times 10^4$ to $1.1 \times 10^5$ is shown. The red line indicates the median $C_D$-values, which range from 1.199 to 1.725. The differences can be explained with the random selection of mussel dropper lines and the unsystematic growth behavior of the attached mussels. As can be seen in Figure 2 and Table 2, the diameter of each mussel dropper line varies.

The arranged data sets reveal that approximately 50 % of each test data points produce an area of interest with reduced variation in $C_D$. This is an indicator for the quality of the representing $C_D$-values taken as median. Generally, the data scattered along the length of these horizontal intervals represents the essential sections of the measurements.

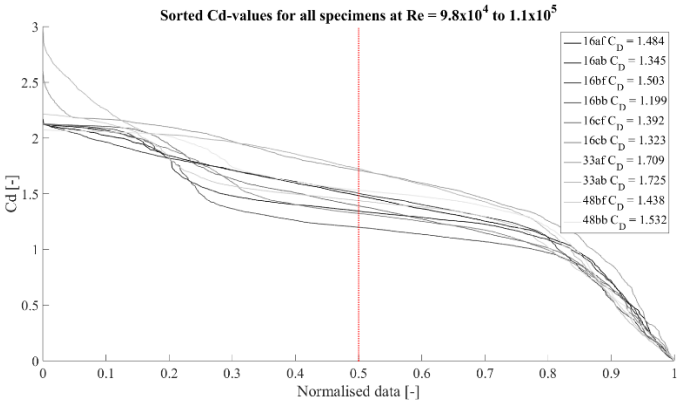


*Figure 5: Normalized and sorted distribution of $C_D$-time series for all specimens tested in-between Reynolds numbers $9.8 \times 10^4$ to $1.1 \times 10^5$. Median values for all conducted tests with specimen 1 (16af, etc.) are listed and emphasized with a red center line.*

The estimated median $C_D$-values are matched to their corresponding Reynolds numbers according to Equation (4) in a subsequent step. The scatter plot for all tested specimens between Reynolds numbers $9.8 \times 10^4$ and $1.1 \times 10^5$, resulting from Figure 5, is depicted in Figure 6. A linear trend of the scattered data around Reynolds number $1.04 \times 10^5$ is apparent and validates the test results in regard to each other.

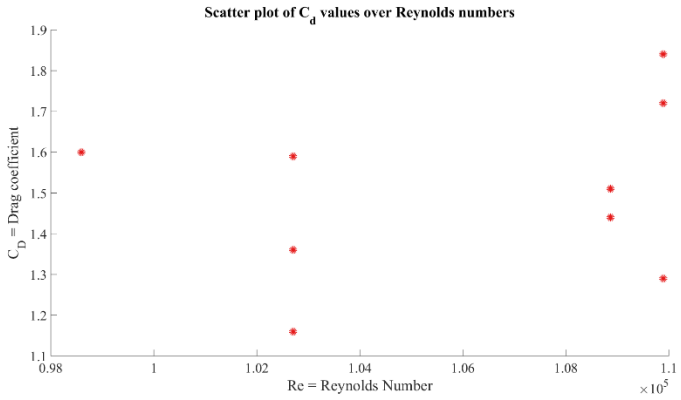


*Figure 6: Scatter plot of median $C_D$-values in-between Reynolds numbers $9.8 \times 10^4$ to $1.1 \times 10^5$.*

All available data is distributed between Reynolds numbers $2.4 \times 10^4$ and $1.1 \times 10^5$ in form of scattered, median $C_D$-values. For a more conclusive comparison to literature and further research several functions are fitted and assessed according to the goodness-of-fit. The goodness-of-fit is evaluated by R-squared ($R^2$) statistics as quantitative measure of how close the data is fitting to regression curves. Polynomial functions of 1st, 3rd and 5th degree are compared to Gaussian equations with 1, 2 and 3 terms as well as to a sum of sine model (S.o.S.) and a weighted smoothing spline (W.S.S.) for comparison. Table 3 gives an overview regarding the $R^2$ values of the compared functions, with all functions and the corresponding equations listed. It is apparent that the linear functions realized as Gaussian and polynomial functions of the first order are a poor fit. The created linear functions are not suitable for the description of the data at hand. The more terms are included in the polynomial and Gaussian equations the more accurately the equation describes the data at hand. Even better results regarding the $R^2$ values could be obtained, however, all options investigated that provide $R^2$ values closer to 1.0 reveal impracticable progressions and are therefore dismissed. The Gaussian equation with 3 terms exhibits the most promising results with a satisfactory $R^2$-value of $R^2 = 0.68$ and a comprehensible contour along the scattered data. All equations mentioned apply only to the Reynolds numbers between $2.4 \times 10^4$ and $1.1 \times 10^5$ and are not applicable for values outside the given range due to generally extreme progressions of spline fittings beyond the data range.

*Table 3: Comparison of fitted lines, with equations used and corresponding $R^2$ values.*

| Function | Equation | $R^2$-value |
|---|---|---|
| Poly. 1.° | f(x) = p1*x + p2 | 0.24 |
| Poly. 3.° | f(x) = p1*x^3 + p2*x^2 + p3*x + p4 | 0.54 |
| Poly. 5.° | f(x) = p1*x^5 + p2*x^4 + p3*x^3 + p4*x^2 + p5*x + p6 | 0.63 |
| Gauss. 1 | f(x) = a1*exp(-((x-b1)/c1)^2) | 0.26 |
| Gauss. 2 | f(x) = a1*exp(-((x-b1)/c1)^2) + a2*exp(-((x-b2)/c2)^2) | 0.56 |
| Gauss. 3 | f(x) = a1*exp(-((x-b1)/c1)^2) + a2*exp(-((x-b2)/c2)^2) + a3*exp(-((x-b3)/c3)^2) | 0.68 |
| S.o.S | f(x) = a1*sin(b1*x+c1) + a2*sin(b2*x+c2) | 0.52 |
| W.S.S. | polynomial computation from smoothing parameter p = 0.9335 | 0.60 |

This concludes the data analysis with the generation of a Gaussian equation that describes the scattered $C_D$-values and the corresponding, velocity-associated Reynolds numbers. The resulting plot is given in Figure 7. The drag coefficient $C_D$ of all tested live-mussel specimens remains relatively stable after an initial drop as shown in Figure 5. The drop occurs from a measured, maximum $C_D$-value of 2.96 at low velocities, corresponding to the Reynolds numbers $2.0 \times 10^4$ to $4.0 \times 10^4$. The stabilization is discernible around a computed median $C_D$-value of 1.59 for the Reynolds numbers $4.0 \times 10^4$ to $1.1 \times 10^5$. Generally, all values are within a $C_D$-range of 1.16 to 2.96. To differentiate between the specimens different markers are used. Specimen 1 with a lower mean diameter $D_i$ is displayed by

diamond shapes while specimen 2 and 3 with comparable mean diameters are represented by plus signs.

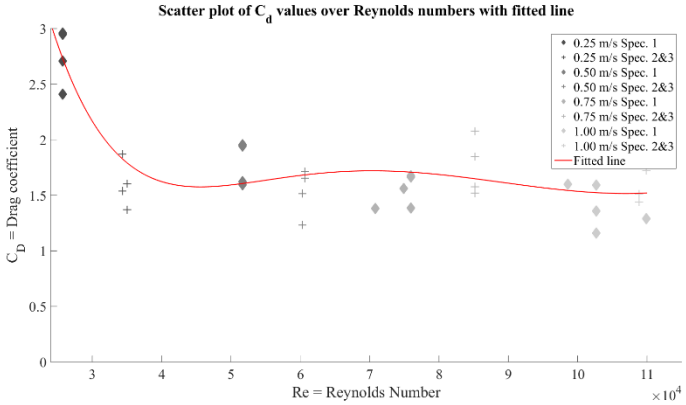


*Figure 7: Scatter plot of $C_D$-values over Reynolds numbers for three different mussel specimens at initially sought velocities of 0.25 m/s, 0.50 m/s, 0.75 m/s and 1.00 m/s.*

## RESULTS AND DISCUSSIONS

The aforementioned drop, or drag crisis, and subsequent stabilization is well documented in literature and generally referred to as critical flow regime. Flow regimes around cylinders with varying $k/D$-values, i.e. relative surface roughness, are commonly researched and can be divided in dependency to the corresponding Reynolds numbers. Definitions vary in literature and for the following discussion the flow regimes will be referred to as "subcritical" flow, "critical" flow, "supercritical" flow and "trans-critical" flow. The subcritical regime is described by a laminar boundary layer flow, while the supercritical and trans-critical regimes are characterized by increasing turbulence in the wake, shear layers and finally in the boundary layer. The critical flow regime is of high interest regarding shifting separation points, reattachments of separation bubbles and the transition from a laminar to a turbulent state. (Schlichting and Gersten, 2017)

It is commonly known, that the relative surface roughness has a large effect on the drag coefficient within chosen Reynolds ranges. Numerous studies for fixed cylinders in flow with varying $k/D$-values show that the rougher the surface area of a cylinder, i.e. described by large $k/D$-values, the lower the Reynolds-numbers associated to the critical flow regime. For example, the critical flow regime of a smooth cylinder occurs in-between Reynolds numbers $2 \times 10^5$ and $5 \times 10^5$ (Faltinsen, 1990). For a rough cylinder with $\frac{k}{D} = \frac{1}{50}$ the critical flow regime is shifted to Reynolds numbers between $0.2 \times 10^5$ and $0.5 \times 10^5$ (Sarpkaya and Isaacson 1976). Consequently a turbulent flow is reached at lower velocities if the roughness increases. A comparison of both cases further indicates that the amplitude and the intensity of the drag crisis is reduced with increasing roughness, indicated by less pronounced drops in the $C_D$ curves. While the smooth cylinder shows a drop of $C_D$ about 1.0, the amplitude drop of the rough cylinder is only around 0.2. This can be reasoned by the missing reattachment of the flow on the rear side of round or oval structures when the turbulence is too high due to the increased roughness.

With regard to the results at hand, it is assumed that the tested mussel dropper lines have an ultra-rough surface with an estimated $\frac{k}{D} \approx \frac{1}{10}$. This is based on the measured single mussels and mean diameter of the tested blue mussel specimens (Landmann et al., 2018). This, in relation to the observations regarding the shift of the critical regime and the reduced intensity of the drag crisis leads to the assumption that for the tested mussel dropper lines the subcritical regime is exceeded at very low velocities corresponding to $Re < 0.2 \times 10^5$. This assumption is supported by data of the underwater camera, which shows bubbles related to turbulent flow at even the lowest test velocities. However, a definite determination of the different flow regimes is part of currently ongoing studies including lower velocities. Higher velocities have little influence on the overall development of the $C_D$-values, since the measured force acting on the mussel dropper lines increases primarily due to the squared velocity. FOT-cleaned force measurements of approximately 10 N can be assumed for the lowest velocities, while nearly 200 N are observed for the mussel dropper lines at the highest tested velocities. The reduced amplitude drop of rough cylinders can be observed for the data at hand only in-between Reynolds numbers of $3.5 \times 10^4$ and $5.0 \times 10^4$. In this context the observed $C_D$-values seem to apply to previous studies. The mussel dropper line can be seen as an ultra-rough surface, which creates turbulence in its wake even at low velocities. The high $C_D$-values as well as the low amplitude of the drop of the measured values suggests that the findings for rough fixed cylinders are comparable to the data at hand. This is also supported by the different specimens and corresponding results. For the specimen 1 with the lowest $D_i$-value (see Table 2) the resulting $C_D$-values are arranged rather higher than the scatter points of specimens 2 and 3. This is visualized with the diamond-shaped scatter points for specimen 1 and the plus sign for specimen 2 and 3 in Figure 7.

To further verify the findings for the mussel dropper lines the naturally occurring variations of the relative surface roughness $k/D$ are tested via a sensitivity study. The effect of a varying characteristic diameter and thus $k/D$-value is presented in Figure 8.

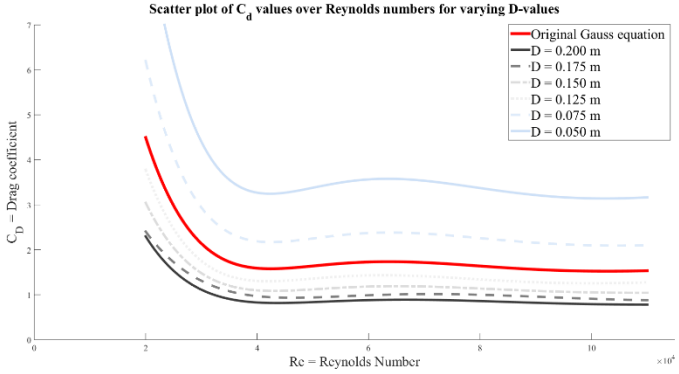


*Figure 8: Comparison of fitted equations in regard to the mean diameter $D_i$.*

Throughout the growing phase of mussels the diameter of the mussel dropper line attached to the suspended long-line systems varies. Furthermore, natural variations occur along the length of the dropper line. This is evident for the selected specimen 1 in Figure 2, where portions of the dropper line are lumped with mussels while other segments show only few attached mussels. Here, the resulting $C_D$-curves are displayed in dependency of $A = L * D_i$ with varying $D_i$'s from 5,0 to 20 cm in 2.5 cm intervals. The 10 cm interval is omitted as the original results with $D_i = 10.31$ cm are plotted in red for reference instead. $L$ remains constant for all computations. The larger $D_i$ is chosen, the lower the $C_D$-values and the less fluctuations are visible in the data. Lower $D_i$-values rapidly shift the regression curve to high $C_D$-values and leads to stronger fluctuations in the data. This is due to the formulation of the drag term and the only changing variable being the mean diameter, while the forces and velocities remain constant. This underlines the relevance of the observations regarding the mean diameter of blue mussel dropper lines.

For the design of suspended aquaculture farms the results indicate that the mean diameter of the mussel as well as fluctuations in density along the mussel dropper lines should be accounted for to achieve efficient designs. Different seizes of artificial surrogate models are currently tested, which show very similar drag characteristics and will be used for further studies and unlimited reproduction of the model tests. The development of surrogates is detailed in Landmann et al. (2018), while the test results will be made available in future publications.

## CONCLUSIONS & OUTLOOK

This work is part of an ongoing research effort related to designing and testing new aquaculture concepts for the usage in high-energy, offshore environments. The aim of the live-mussel testing and the evaluation of the gathered data is to identify drag, inertia and turbulence characteristics of mussel dropper lines, as these will most likely be an imperative part of future offshore bivalve aquaculture. A better understanding of the forces acting on suspended long-line systems enables optimized and cost efficient systems. The knowledge gathered for such a development is based on full-scale physical model tests carried out in state of the art test facilities supplemented by numerical calculations.

The obtained results regarding drag characteristics can be summarized as follows:

- Estimated $C_D$-values for the individual blue mussel specimens range between 1.16 and 2.96 for the tested Reynolds numbers.
- The tested mussel specimens can be assumed to be ultra-rough surfaces $\left(\frac{k}{D} < \frac{1}{10}\right)$.
- Higher velocities reveal little changes in the magnitude of the $C_D$-value and after the initial drop the $C_D$-value has shown to be rather constant about 1.6.
- The diameter influences the $C_D$-curve characteristics.

The results of this paper will be incorporated in further projects focusing on the testing of generated mussel surrogate models and on the scale effects of the mentioned surrogates. The surrogates will be evaluated regarding the investigated $C_D$-values as well as in regard to other inertia- and turbulence characteristics of mussel dropper lines. The pertaining investigations will be made available in upcoming research.

## ACKNOWLEDGMENTS

This Research has been supported with funding from the New Zealand Ministry of Business, Innovation and Employment through Cawthron Institute project CAWX1607. Furthermore, the authors gratefully acknowledge the support of Prof. Dr. Bela H. Buck for providing us with insight into bivalves, from Dr.-Ing. Jens-André Paffenholz of the Geodetic Institute Hannover during 3D-scanning, from Dr. Tim Staufenberger for providing us with the mussel specimens and from Kevin Heathman on behalf of the Cawthron Institute for support regarding bivalve characteristics.

## REFERENCES

Achenbach, E.; 1971. Influence of surface roughness on the cross-flow around a circular cylinder. J. Fluid Mech., 46, 321-35.

Buck, B.H and Krause, G.; 2013. Short expertise on the potential combination of aquaculture with marine-based renewable energy systems. SeaKult-Sustainable Futures in the Marine Realm. Expertise für das WBGU-Hauptgutachten „Welt im Wandel: Menschheitserbe Meer“. 58.

Buck, B.H.; Ebeling, M.W.; Michler-Cieluch, T.; 2010. Mussel cultivation as a co-use in offshore wind farms: potential and economic feasibility, *Aquaculture Economics & Management*, 14: 4, 255 — 281

Carlberg, L.K. and Christensen, E.D.; 2015. Go offshore—Combining food and energy production. DTU Mechanical Engineering, *Technical University of Denmark*. 48

Constantinescu, G.; Miyawaki, S.; Liao, Q.; 2013. Flow and Turbulence Structure past a Cluster of Freshwater Mussels. Journal of Hydraulic Engineering. 139, 4 , 347 - 358

Faltinsen, O.M., 1990. SEA LOADS ON SHIPS AND OFFSHORE STRUCTURES, *CAMBRIDGE UNIVERSITY PRESS, 174 – 222*

FAO, 2016. The State of World Fisheries and Aquaculture 2016 - Contributing to food security and nutrition for all. 1, 170 – 188.

FAO, 2017. Cultured Aquatic Species Information Programme: Mytilus edulis (Linnaeus, 1758). *FAO Fisheries and Aquaculture Department* [online]. Rome. Updated 1 January 2004. [Cited 24 November 2017].

Gansel, LC; Endresen, P.; Steinhovden, K., et al., 2017. Drag on Nets Fouled With Blue Mussel (Mytilus Edulis) and Sugar Kelp (Saccharina Latissima) and Parameterization of Fouling. ASME. International Conference on Offshore Mechanics and Arctic Engineering, *Volume 6: Ocean Space Utilization* ():V006T05A008. doi:10.1115/OMAE2017-62030.

Goseberg, N.; Chambers, M.D.; Heasman, K.; Fredriksson, D.; Fredheim, A.; Schlurmann, T.; 2017. Technological Approaches to Longline- and Cage-Based Aquaculture in Open Ocean Environments, *Aquaculture Perspective of Multi-Use Sites in the Open Ocean*, 71-95

Hildebrandt, A., Sparboom, U., Oumeraci, H. 2008. Wave forces on groups of slender cylinders in comparison to an isolated cylinder due to non-breaking waves. *Coastal Engineering Conference, 31st ICCE*

Hildebrandt, A., Sriram, V. 2014. Pressure distribution and vortex shedding around a cylinder due to a steep wave at the onset of breaking from physical and numerical modeling. *Proc. 24th ISOPE*

 

Lagerveld, S.; Röckmann, C.; Scholl, M.; 2014. Combining offshore wind energy and large-scale mussel farming: Background and technical, ecological and economic considerations. IMARES Wageningen UR, *Report C056/14*. 117

Landmann, J.; Ongsiek, T.; Goseberg, N.; Hildebrandt, A.; 2018. INVESTIGATING DRAG AND INERTIA CHARACTERISTICS OF FULL-SCALE BLUE MUSSEL DROPPER LINES, *COASTLAB18* - Manuscript submitted for publication.

McVey, J.P.; 1996. Open ocean aquaculture. Proceedings of an international conference, Overview of offshore aquaculture. Polk, M. (ed) *New Hampshire-Maine Sea Grant College Program No. UNHMP-CP-SG-96-9*, 1 -4

Morison J. R., O'Brien M. D., Johnson J. W., and Schaaf S. A., 1950. The force exerted by surface waves on piles. *Petrol Trans AIME*. 189.

Sansom, B.J.; Atkinson, J.F.; Bennett, S.J.; 2017. Modulation of near-bed hydrodynamics by freshwater mussels in an experimental channel. *Hydrobilologia*, 1-15

Sarpkaya, T. and Isaacson, T.; 1981. Mechanics of Wave Forces on Offshore Structures. Van Nostrand Reinhold Company

Schlichting, H.; Gersten, K.; 2017. Boundary-Layer Theory. XXVIII, 805, *Springer Berlin Heidelberg* 9, 3 – 48

Welzel, M., Kreklow, T., Schlurmann, T., Hildebrandt, A. 2016. Excitation and dynamic responses of jacket structures in regular waves for offshore installation. *Coastal Engineering Conference, 35th ICCE*

van den Burg, S.W.K.; Stuiver, M.; Veenstra, F.A.; Bikker, P.; Lopez-Contreras, A.M.; Palstra, A.P.; 2013. Triple P review of the feasibility of sustainable offshore seaweed production in the North Sea. Lei Wageningen UR. *Lei Reports* 13, 77, 105